Electric-field-induced deformation dynamics of a single nematic disclination

Angela Vella, Romuald Intartaglia, Christophe Blanc, Ivan I. Smalyukh, Oleg D. Lavrentovich, Maurizio Nobili

Electric-field-induced deformation dynamics of a single nematic disclination

Angela Vella,[1] Romuald Intartaglia,[1] Christophe Blanc,[1] Ivan I. Smalyukh,[2] Oleg D. Lavrentovich,[2] and Maurizio Nobili[1]
[1]*GDPC (UMR 5581) CNRS, Université de Montpellier-II, CC026, Place Eugéne Bataillon, F-34095 Montpellier Cedex 05, France*
[2]*Chemical Physics Interdisciplinary Program and Liquid Crystal Institute, Kent State University, Kent, Ohio 44242, USA*
(Received 7 May 2004; revised manuscript received 11 November 2004; published 17 June 2005)

Disclinations in nematic liquid crystals usually adopt a straight shape in order to minimize their elastic energy. Once created in the course of a nonequilibrium process such as a temperature quench from the isotropic to the nematic phase, the topologically stable disclinations of half-integer strength either annihilate each other in pairs of opposite strength or form topologically unstable disclinations of integer strength. In this article, we demonstrate that the annihilation process can be inhibited and the defects can be deformed by an applied electric field. We study the disclination lines in the deep uniaxial nematic phase, located at the boundary between two different types of walls, the so-called π wall (a planar soliton stabilized by the surface anchoring) and the Brochard-Léger (BL) wall stabilized by the applied electric field. By changing the electric voltage, one can control the energy of director deformations associated with the two walls and thus control the deformation and dynamics of the disclination line. At small voltages, the disclinations are straight lines connecting the opposite plates of the cell, located at the two ends of the π walls. The π walls tend to shrink. When the voltage increases above E_F, the Fréedericksz threshold, the BL walls appear and connect pairs of disclinations along a path complementary to the π wall. At $E>2E_F$, the BL walls store sufficient energy to prevent shrinking of the π walls. Reconstruction of the three-dimensional director configuration using a fluorescent confocal polarizing microscopy demonstrates that the disclinations are strongly bent in the region between the π and the BL walls. The distortions and the related dynamics are associated with the transformation of the BL wall into two surface disclination lines; we characterize it experimentally as a function of the applied electric field, the cell thickness, and the sample temperature. A simple model captures the essential details of the experimental data.

DOI: 10.1103/PhysRevE.71.061705 PACS number(s): 61.30.Jf, 61.30.Hn, 61.72.Cc

I. INTRODUCTION

The nematic phase of liquid crystals is characterized by a uniaxial orientational order. The nematic order is associated with a unit director $\hat{\mathbf{n}}=-\hat{\mathbf{n}}$ representing the average direction of the elongated liquid crystal molecules. This orientational order can be broken locally on a point or along a line, generating a singularity for the director field. In analogy with the dislocations in a crystal, nematic line defects are named *disclinations*. The disclinations are topological objects and are often classified according to their strength which can be integer or half integer [1,2]. The half-integer disclinations are truly topologically stable objects that cannot be transformed into a uniform state by any smooth transformation of the associated director field; however, they all belong to the same topological class and can be transformed into each other at least when the sample boundary do not create any obstacles for such transformation. Integer strength lines are not topologically stable and relax into nonsingular configurations [3,4]. The disclinations carry the energy of elastic director distortions outside the singular core and a special energy associated with the singular core itself at which the order parameter is different from the regular nematic one. Such defects can be easily obtained in a thermotropic liquid crystal by a rapid quench from the high symmetry isotropic phase to the lower symmetry nematic phase or by a pressure jump [5]. Alternative routes to create disclinations are the use of particular frustrated geometries [6,7] or the application of external fields in a process named *pincement*. In this process, a Brochard-Léger (BL) wall [8,9] is converted into two opposite sign disclinations when the destabilizing electric field is larger than a critical value $E_C \approx 2E_F$ (where E_F is the Fréedericksz threshold) [10]. By increasing the destabilizing electric field amplitude, the elastic energy cost of the BL wall increases. Two disclinations appear when the BL wall energy reaches the nucleation energy of the disclinations pair. The BL-wall–disclination conversion dynamics has been recently measured in a free standing nematic film submitted to an electric field [11].

The disclination dynamics has also been studied in frustrated geometries. In one of these geometries disclinations are induced by antagonistic boundary conditions [12] and are moved under the effect of an electric field [6]. In another geometry disclination pairs are nucleated by a rapid quench from the isotropic phase in a strongly confined geometry of a few micrometers thickness. The annihilation dynamics is driven by the anchoring energy on the confinement substrates [7]. In both these systems, straight defect lines are induced by the particular chosen geometries and the boundary conditions.

The energy of a straight disclination is proportional to its length [3]. The energy of a curved line, in first approximation, is also proportional to its length [4]. A curved line thus has a tendency to straighten, in order to decrease its length. This tendency can be described in the terms of a line tension, which is the ratio of the variation of elastic energy to the variation in length [4]. Under certain conditions, line defects in the nematic bulk deviate from the straight line and develop a zigzag shape. This instability is induced by the an-

isotropy of the nematic elasticity. The increased total disclination length is over-compensated by the energy decrease due to the conversion of the high energy splay-bend deformation into the lower energy twist [13–15].

As far as we know, the deformation dynamics of an isolated disclination remains largely unexplored. The aim of this paper is to describe the deformation dynamics of a single disclination under an external electric field.

Straight disclinations orthogonal to the cell parallel plates are formed by a rapid quench from the isotropic phase. The nematic director in the cell is uniformly oriented along the parallel planar easy axes of the two substrates. The elastic energy excess, due to the presence of the disclinations, and the related excess of anchoring energy on the confinement substrates force the line defects to annihilate by pairs [7]. If a destabilizing electric field parallel to the disclinations is applied, the dynamics of annihilation is strongly modified. At electric fields E larger than the Frederiks threshold E_F, segments of BL walls appear and connect disclinations of opposite signs. The annihilation is more and more dampened for increasing fields and even stops at a critical field $E_C \approx 2E_F$ for which the two defects are immobilized. In the explored field range $E \approx E_C$, two different dynamical regimes are observed.

At temperatures T close to the isotropic-nematic transition temperature T_{NI} ($\Delta T = T_{NI} - T < 2$ °C), the line defect is only weakly deformed by the electric field. It moves as a whole by remaining almost straight and orthogonal to the substrates. In this regime, the line displacement is controlled by the surface energy change, and displays a complex dynamics. The study of such a regime will be published in a forthcoming paper.

In the second regime, at lower temperature, the line remains pinned with its two ends on each substrates. The dynamics does not imply surface changes but only bulk deformation. Under the electric field, the line bends. In this paper we measure the bending profile and the related dynamics as a function of the electric field amplitude, the sample thickness, and the temperature. A simple elastic model is proposed which is in a good agreement with the experimental results.

The paper is organized as follows. Section II is devoted to the experimental setup and general observations. Section III details the quantitative study of the half-integer disclination bending dynamic. In Sec. IV we present an elastic model explaining the experimental results. Finally the conclusions are drawn in Sec. V.

II. EXPERIMENT

A. Experimental setup

A 5CB (4-cyano-4-*n*-pentylbiphenyl from Synthon) film is sandwiched between two parallel glass plates covered by a thin (50 nm) indium tin oxide (ITO) conductive coating. Each glass plate is covered by a 150 Å thick SiO layer evaporated at a 60° incident angle in order to obtain a homogeneous planar anchoring. The glass plates are then assembled with parallel easy axes. The cell thickness d is fixed by means of Mylar spacers in the range 3–50 μm, and measured before filling by using a spectrophotometer. A 10% relative thickness variation is measured on the whole cell.

Samples are observed under a polarizing microscope. The temperature is controlled by an oven (INSTEC STC200D) (accuracy of 0.1 °C). The difference in temperature $\Delta T = T_{NI} - T$ (T is the sample temperature and $T_{NI} = 35.3$ °C is the 5CB clearing temperature) is tuned between 2 and 7.3 °C during our experiments. An ac electric field perpendicular to the plates can be applied to the sample. To avoid electrohydrodynamic instabilities, the ac generator operates at a frequency of 10 kHz. This frequency is two orders of magnitude larger than the 5CB dielectric relaxation frequency [16]. The microscope is equipped with a fast charge-coupled device (CCD) camera (Pulnix TM-6703) and a PC frame grabber. The acquisition system is able to store up to 100 frames/s.

The optical measurements have been completed by observations under a fluorescent confocal polarizing microscope (FCPM) [17,18]. This technique allows one to determine the director orientation along the depth of the cell. The large birefringence of 5CB decreases the FCPM resolution preventing any quantitative measurement of the director field. To obtain a better resolution, we have replaced 5CB with MLC6815 (purchased from EM Industries) which has small birefringence $\Delta n \approx 0.05$, positive dielectric anisotropy like 5CB, and clearing point $T_{NI} = 67$ °C. For the FCPM observations, the material is doped with a very small amount (0.01 wt %) of fluorescent dye 5-decyl-4,4-difluoro-4-bora-3*a*,4*a*-diaza-*s*-indacene-3-propionic acid (C_{10}-BODIPY500/510C_3, purchased from Molecular Probes). To minimize spherical aberrations in FCPM studies with an immersion oil objective, we used glass substrates of thickness 0.15 mm with a refractive index 1.52. The FCPM set up was assembled on the basis of an Olympus Fluoview BX-50 reflective-mode confocal microscope. The Ar laser (488 nm, beam power $<$1mW) was used for excitation. The fluorescent light was detected by a photomultiplier tube in the spectral region 510–550 nm as selected by interference filters in the detection channel. We used an immersion oil objective 60× (numerical aperture 1.4) which allowed for the FCPM studies with resolution ≈ 1 μm in radial as well as axial directions. The very same polarizing element determines the linear polarization direction $\hat{\mathbf{P}}$ of both the excitation beam and the detected fluorescent light. The FCPM signal results from a sequence of absorption and emission. It strongly depends on the angle δ between the transition dipole (parallel to the local director in our system) and the linear polarizer. In the case of circular polarization, δ corresponds to the angle between the plane of observations (the plane normal to the optical axis of the microscope) and the director. In both cases, the fluorescence signal is proportional to $\cos^4 \delta$, as both as absorption and emission follow the dependency $\sim \cos^2 \delta$ [18]. For linear polarization, the maximum fluorescence signal is when $\hat{\mathbf{n}} \| \hat{\mathbf{P}}$ and minimum when $\hat{\mathbf{n}} \perp \hat{\mathbf{P}}$. For circular polarization, the strongest fluorescent signal is obtained when the director is in the plane of observation, and minimum when it is along the optical axis of microscope (along the cell normal). The FCPM intensity patterns in linear and circular polarization were used to map the three-dimensional director structures.

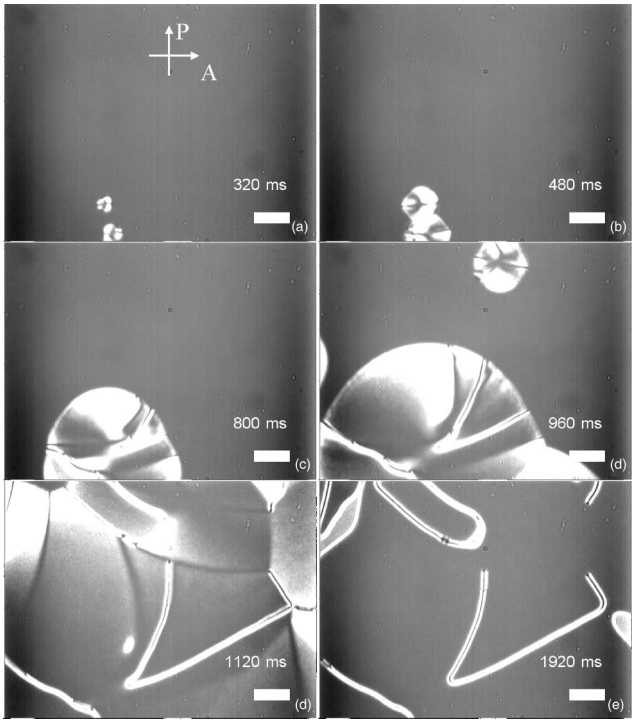

FIG. 1. Nucleation of the nematic phase of 5CB after a quench from the isotropic phase into a cell with planar anchoring and formation of disclinations connected by π walls (see text). Thickness of the cell 11 μm. Bar 40 μm. $T=33.5\,^{\circ}$C.

B. General observations

The sample in the nematic phase is aligned along the two parallel easy axes at the chosen temperature $T=T_{NI}-\Delta T$. A short pulse of hot air is injected into the oven, which increases the sample temperature above T_{NI}. The sample becomes isotropic but after a few seconds the temperature decreases and droplets of nematic phase nucleate and grow (Fig. 1). Depending on the director orientation on the surface of neighboring droplets, disclinations may appear when droplets coalesce. Figure 2 shows a top view of a $\{-1/2, +1/2\}$ disclination pair. Two superposed surface walls are also created between them during this process. Note that these walls are not necessarily straight. The disclinations are situated at the ends of the surface walls and appear as points in a top view (they are parallel to the light path and orthogonal to the two surfaces). This orientation is induced by the confinement and the strong planar anchoring conditions. Each surface wall corresponds to a continuous π-rotation of the director on the surface as proved by the presence of two bright fringes under crossed polarizers in Fig. 2. As the director turns by π, between two equivalent states, these walls are topologically stable, as long as the in-plane surface anchoring remains nonzero; they represent what are called the planar solitons [19] or the π walls. The annihilation dynamics of pair of opposite sign disclinations is driven by the elastic energy excess associated with these π walls [7].

If an electric field parallel to the disclinations is applied before their annihilation, their dynamics is strongly affected. Above the Fréedericksz threshold E_F, a splay-bend director

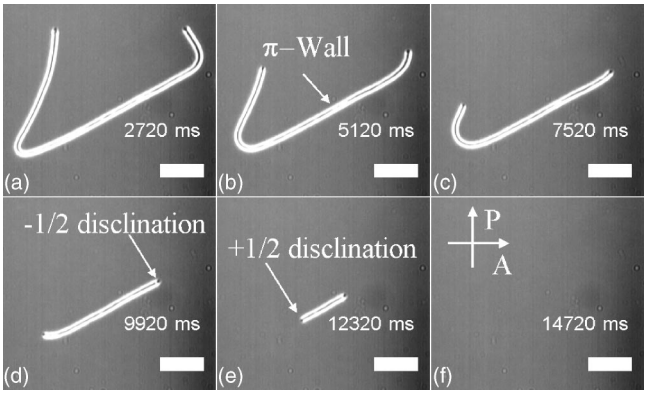

FIG. 2. Annihilation of a pair of $\pm 1/2$ disclinations under crossed polarizers (electric field off). The disclinations are situated on the end tips of the topological wall (the two bright fringes), whose formation is shown in Fig. 1. Each end tip represents the projection of a line defect orthogonal to the substrates. Cell thickness is 11 μm. Bar 40 μm. $T=33.5\,^{\circ}$C.

distortion develops in the cell. Due to the quadratic dielectric coupling $(\mathbf{E}\cdot\hat{\mathbf{n}})^2$, the equilibrium distorted state is twofold degenerate. Domains characterized by one of the two equilibrium textures appear. Two adjacent domains are separated by a bulk distortion wall called a Brochard-Léger wall [8,9]. In the presence of disclination pairs, segments of BL wall connect defects of opposite charge (see Fig. 3(b)]. In the case of an isolated pair, a mixed loop made by a BL wall and a π wall frequently forms [Fig. 3(d)].

The annihilation process is inhibited for a critical field E_C ($E_C \approx 2E_F$). Figure 4 shows the defect behavior when $E < E_C$: the π wall retracts in favor of the BL wall [11,20]. During the relaxation, the defect lines remain almost straight and orthogonal to the substrates, which is similar to the relaxation without electric field [7]. After the defect annihilation, in the case of a single mixed loop, this latter is transformed into a regular BL wall [8,9] [see Fig. 4(d)], which finally relaxes.

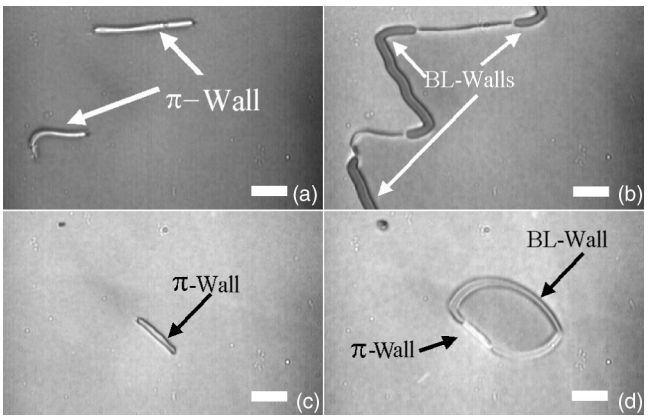

FIG. 3. $+1/2, -1/2$ line defect pairs are connected by a π wall without electric field (a)–(c). Above the Fréedericksz transition, Brochard-Léger walls appear between different pairs (b) or connect defects of the same pair, thus forming a mixed loop (d). Cell thickness is 11 μm. Bar 40 μm. $T=33.5\,^{\circ}$C. Polarizers slightly uncrossed.

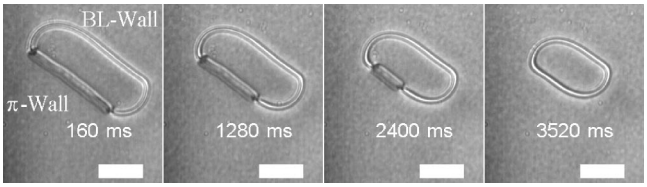

FIG. 4. Annihilation of a pair of ±1/2 disclinations in the presence of an electric field $E=0.2$ V μm^{-1}. Bar 40 μm. Thickness of sample 11 μm. $\Delta T \approx 3$ °C.

At high field ($E > E_C$) and at high temperature ($\Delta T < 2$ °C), the defect velocity is reversed with respect to the low field case: the BL wall is now converted to a π wall [10,11] as shown in Fig. 5. The final state after the defect annihilation consists in two surface π loops, one on each surface [Fig. 5(d)]. Differently from a BL loop, these loops do not disappear after the electric field is switched off. In the two regimes presented so far (low field or high temperature), the two defect ends move with respect to the substrates and the elastic driving force depends on the anchoring energy.

At low temperature ($\Delta T > 2$ °C) a different type of dynamics is observed. A region β appears between the π and the BL walls as shown in Fig. 6. This β region corresponds to a strong deformation of the initially straight disclination (see Figs. 7 and 8). The BL wall length decreases in favor of the β region, keeping unchanged the π wall length.

The rest of the paper is dedicated to the study of the single disclination deformation (region β) and its dynamical behavior. In particular, the line is first bent with an electric field larger than the critical one. Then, the bending (positive velocity) and the unbending (negative velocity) dynamic are measured as function of the field. Because segments of BL walls move very easily and BL loops shrink rapidly (they involve only bulk deformation), the quantitative study of the dynamics of a ±1/2 disclination along a BL wall is usually affected by the lateral motion of the wall. We therefore observe its motion along very large mixed loops (mean radius $R \gg 100$ μm). The almost straight BL walls (see Fig. 6) are indeed motionless compared to the typical disclinations dynamics. The digitized images of the motion are then analyzed with a home-made program in order to obtain the position of the defect along the wall as a function of time.

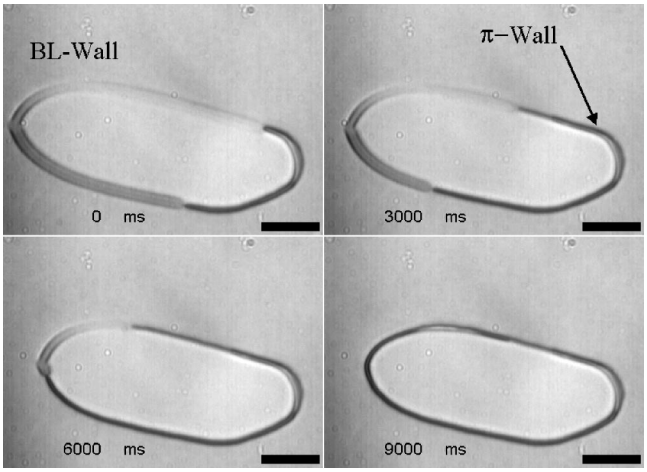

FIG. 5. Annihilation of a pair of ±1/2 disclinations in a mixed loop for large electric fields ($E > E_C$) and high temperature ($\Delta T < 2$ °C. The BL wall disappears and two stable π loops are formed at the end (one on each surface). Bar 40 μm. Thickness of sample 11 μm. $\Delta T \approx 1$ °C.

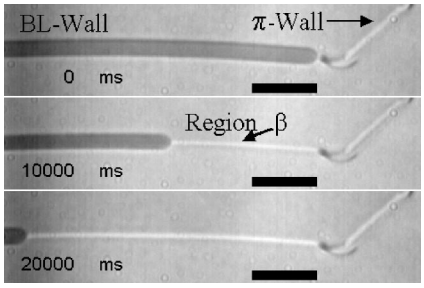

FIG. 6. Appearance of a region β between the π wall and the BL wall for electric fields larger than E_C. This region increases at the expense of the BL wall. Cell thickness is 11 μm. Bar 40 μm. $\Delta T = 3$ °C.

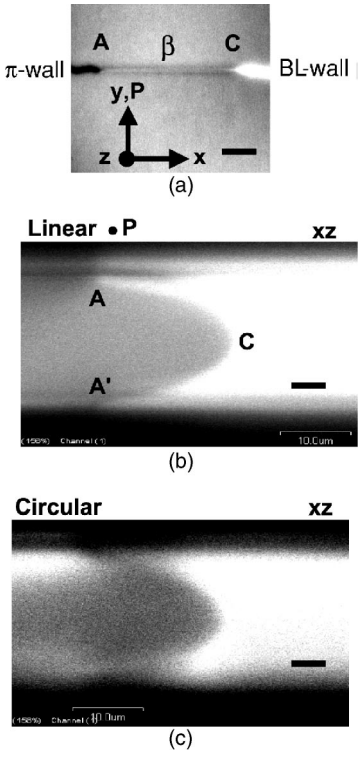

FIG. 7. Characterization of a +1/2 disclination bending behavior under electric field by FCPM. The surface easy axes are parallel to the y axis. (a) xy scan in the plane $z=d/2$ (middle of the cell). We used linear polarization $\hat{\mathbf{P}}$ parallel to the $\hat{\mathbf{y}}$ axis. The region β between the π and BL walls is the disclination bending region. (b) xz scan in the plane containing the π and BL walls. The polarization is the same as in (a). C is the inversion point of the bending deformation of the disclination. (c) xz scan in the same region as (b) with circular polarization. The bar in each picture is 5 μm. T=25 °C.

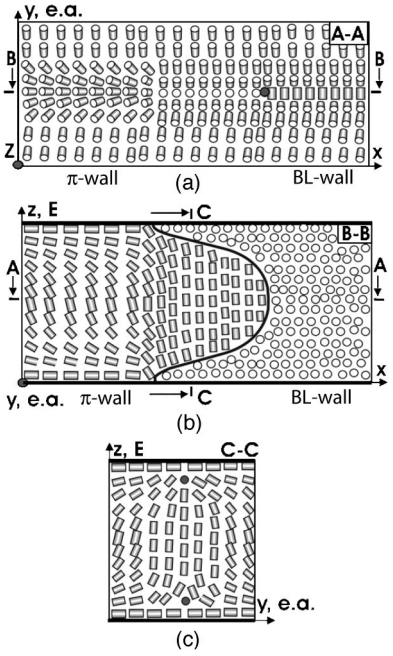

FIG. 8. Different views of the director field reconstructed from the FCPM scans in Fig. 7. (a) Top view corresponding to Fig. 7(a). (b) Side view in the *xz* plane containing the π wall, the bent disclination, and the BL wall. (c) Side view in the *yz* plane corresponding to the bent disclination region. The easy axis (e.a.) is along the *y* axis.

III. HALF-INTEGER DISCLINATION BENDING UNDER AN EXTERNAL ELECTRIC FIELD

Figure 7 shows a typical behavior of +1/2 disclination under an external electric field measured by FCPM. To characterize this region by the FCPM technique, we freeze this texture (once obtained at $E>E_C$) by decreasing the field to $E=E_C$. Figure 7(a) shows an *xy* scan. The polarization of the probing light has been chosen along the *y* axis (easy axis) in order to increase the contrast between the π and BL walls. The large fluorescent intensity from the BL wall proves that the director in this region is oriented in the *yz* plane with a strong component along the *y* axis. In contrast, the relatively low intensity in the region corresponding to the π wall is due to a director oriented in the *xz* plane, perpendicular to the polarization [see sketch in Figs. 8(a) and 8(b)]. In Fig. 7(a), a π wall on the left is connected to a BL wall on the right by a region β. The region β lies between the points *A* and *C*. Figure 7(b) shows an *xz* scan in the plane defined by the π and BL wall centers (*x* axis), and by the normal to the cell (*z* axis). The linear polarization of the probing light is the same as in Fig. 7(a). The π and BL walls are clearly seen as separated by a bent disclination line. The line is pinned at the point *A* of the upper surface and it is bent into the cell bulk. The point *C* is the apex of the line deformation. The region β in Fig. 7(a) corresponds then to the bending of the +1/2 disclination. Figure 7(c) shows an *xz* scan obtained with a circularly polarized excitation beam. The BL wall appears bright proving that the director at the center of the BL wall is oriented in the polarization plane. The region corresponding to the π wall appears almost dark in the middle of the cell

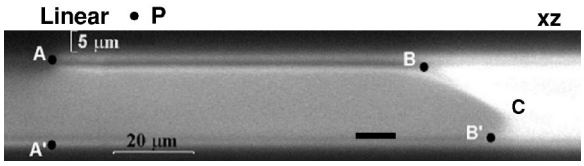

FIG. 9. FCPM *xz* scan of a stretched disclination. Note that the defect line remains at a few micrometers from the surfaces in the *AB* and $A'B'$ parts. The bar is 10 μm. $T=25$ °C.

and bright close to the upper surface. On the π wall, the director in the sample bulk is almost parallel to the electric field (*z* axis), while near the substrates, $\hat{\mathbf{n}}$ remains horizontal due to the imposed planar anchoring.

The asymmetry of the intensity profile with respect to the middle of the cell in this region is an experimental artefact. The polarized beam arriving on the bottom plate from above is defocused by the propagation in the anisotropic nematic. Consequently the image of the director field at the bottom plate is blurred and the fluorescent intensity differs somewhat from the one close to the top plate. Figure 8 shows three different views of the director field reconstructed from the FCPM scans in Fig. 7.

When a larger field is applied ($E>E_C$), the distortion of the defect line increases (its ends remain pinned on the surfaces). The length of the region β can reach very large values, as large as a few hundred micrometers. The line is parallel and very close (a few micrometers) to the upper surface going from the point *A* to the point *B* as shown in Fig. 9. It then bends in the bulk from *B* to *C* and from *C* to B'. Finally the part $B'A'$ is also parallel and close to the lower surface.

The dynamics of the inversion point *C* has been measured versus the amplitude of the electric field, the cell thickness, and the sample temperature. The measurements have been done with the following procedure. We first apply an electric field $E>E_C$ to bend the line defect as in Fig. 9. Once the line is deformed, we immobilize it by decreasing the electric field amplitude to the stabilization value $E=E_C$. A typical working length of the β region is a few hundred micrometers. The line inversion point *C* dynamics is then measured by tuning

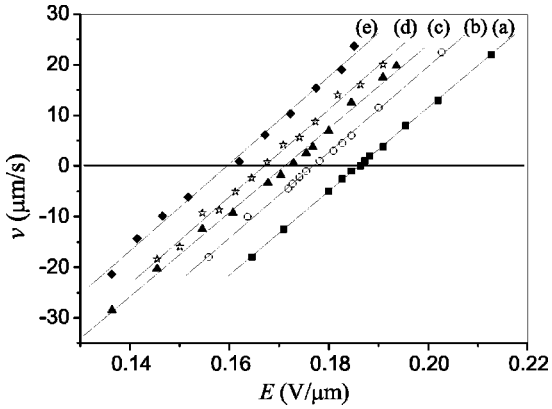

FIG. 10. The velocity of the inversion point *C* versus the effective electric field for different sample temperature: $\Delta T=$ (a) 7.3; (b) 4.3; (c) 3.6; (d) 3.2; and (e) 2.3 °C. The sample thickness is 11 μm. The plain lines are the best fit with Eq. (16). $T_{NI}=35.3$ °C.

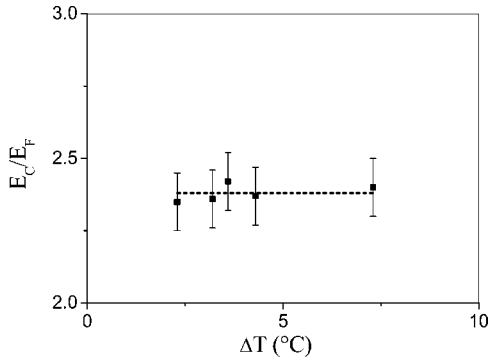

FIG. 11. $\tilde{E}=E_C/E_F$ as a function of $\Delta T=35.3\ ^\circ C-T$ for a cell thickness $d=11\ \mu$m. The points are the experimental data and the line is the average $\tilde{E}$ value.

the electric field amplitude around E_C. Each measurement begins 1 s after the electric field amplitude change. The motion is uniform. Figure 10 shows the dependence of the C velocity v on the effective applied field E for different sample temperatures. Note that v depends linearly on the field in the studied range of values. The threshold field E_C decreases with increasing temperature whereas the velocity susceptibility to the electric field $\alpha=dv/dE$ is almost temperature independent.

In Fig. 11 the critical field $\tilde{E}_C=E_C/E_F$ normalized to the Fréedericksz field E_F is plotted versus ΔT. E_C has been obtained from the best fit of the data points in Fig. 10 whereas E_F has been directly measured on the same cell region in order to minimize the errors due to the cell thickness inhomogeneities.

The ratio $\tilde{E}_C$ is found independent of the sample temperature, which shows that the stabilization field scales as the Fréedericksz field when the temperature changes. Concerning the dependence on the cell thickness, Fig. 12 shows that $\tilde{E}_C$ increases with increasing thickness in the 10–50 μm range.

The velocity susceptibility to the electric field α is however almost independent of the thickness d and the sample temperature, as shown in Figs. 13 and 14, respectively.

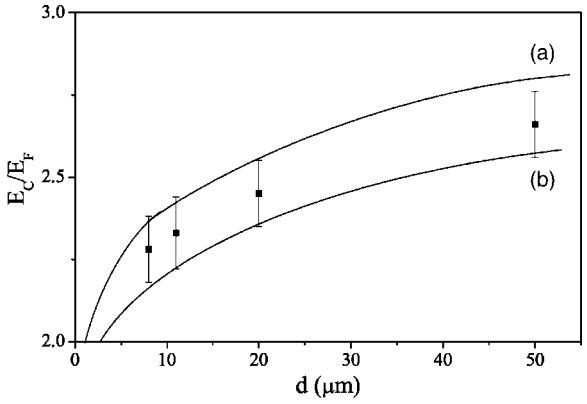

FIG. 12. $\tilde{E}=E_C/E_F$ vs the cell thickness at $\Delta T=2.3\ ^\circ$C. The points are the experimental data and the curves represent the expected theoretical dependence [Eq. (14)] with $\xi=3.3$ (a) and 1.2 nm (b).

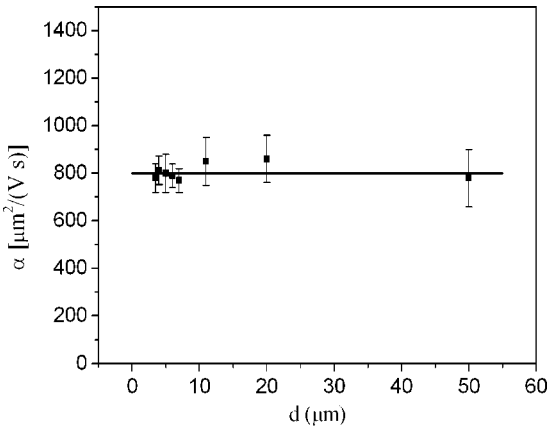

FIG. 13. Velocity susceptibility to the electric field $\alpha=dv/dE$ versus the sample thickness for $\Delta T=2.3\ ^\circ$C. The points are the experimental data; the plain line represents the model prediction [Eq. (18)] for $b=1.22$.

IV. MODEL

In the regime of large disclination deformations presented in Sec. III, the experimental line profile is similar to the one shown in Fig. 9. The line is therefore composed of three main parts: the first one AB is parallel and very close to the upper substrate, the second one BB' is almost perpendicular to the surfaces and is weakly bent, and, finally, the third one $B'A'$ (barely visible in Fig. 9) is close and parallel to the lower surface. Experimentally we observe the part BB' remains weakly bent during the stretching and unstretching of the line. To model our system, we assume the part BB' changes only its location but not its shape and the segments AB and $A'B'$ change their length. In this approximation, the disclination deformation is driven by a conversion of the BL wall elastic energy into the energy of two parallel disclinations. Applying the virtual work principle, the driving elastic force on the disclination F_{el} is given by

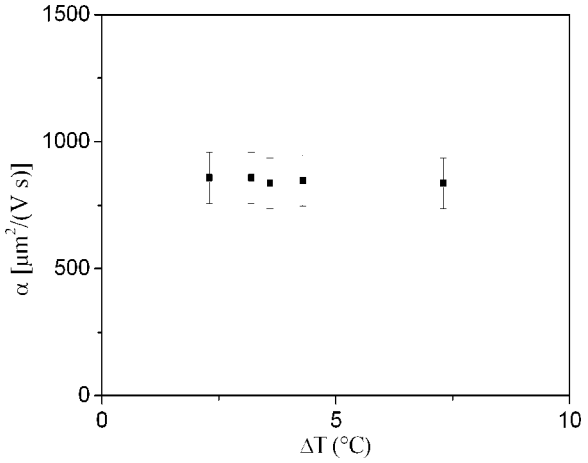

FIG. 14. Velocity susceptibility to the electric field $\alpha=dv/dE$ versus $\Delta T=35.3\ ^\circ\text{C}-T$ for $d=11\ \mu$m.

$$F_{el} = U_\beta - U_{BL}, \tag{1}$$

where U_β and U_{BL} are the elastic energies per unit length along the x axis of the disclination bent region β and the BL wall γ, respectively. To compute U_{BL} we have used the one-elastic-contant approximation ($K=K_1=K_2=K_3$). In this approximation the nematic director $\hat{\mathbf{n}}$ is in the yz plane defined by the direction of the electric field ($\hat{\mathbf{z}}$ axis) and the orientation of the surface easy axis ($\hat{\mathbf{y}}$ axis). We denote by θ the angle formed by $\mathbf{n}$ and $\hat{\mathbf{y}}$. Assuming that θ is small, we expand it in Fourier series and keep the first term [21]

$$\theta(y,z) = \theta_m(y)\sin\left(\frac{\pi z}{d}\right). \tag{2}$$

The elastic energy per unit length of the BL wall, $\mathcal{F}_1$, is given at first order by

$$\mathcal{F}_1 = \int\int \left\{ \frac{K}{2}\left[\left(\frac{\partial\theta}{\partial z}\right)^2 + \left(\frac{\partial\theta}{\partial y}\right)^2 \right] - \frac{\epsilon_0\epsilon_a}{2}E^2\left(\theta^2 - \frac{\theta^4}{3}\right) \right\} dz\, dy, \tag{3}$$

where ϵ_0 is the vacuum dielectric permeability and ϵ_a is the dielectric anisotropy. In Eq. (3) we have assumed $\theta \ll 1$ and we have consequently developed the dielectric term. In this limit the equilibrium director orientation is given by

$$\theta_m(y) = \sqrt{2\left[1 - \left(\frac{1}{\tilde{E}}\right)^2\right]}\tanh\left(\frac{y}{\ell}\right), \tag{4}$$

where $\tilde{E}=E/E_F$, $E_F=\sqrt{K/\epsilon_0\epsilon_a}(\pi/d)$, and

$$\ell = \frac{d}{\pi}\sqrt{\frac{2}{(\tilde{E}^2-1)}}. \tag{5}$$

By substituting Eq. (4) in Eq. (3), $\mathcal{F}_1$ becomes

$$\mathcal{F}_1 = \frac{K\pi^2}{4d}\frac{(\tilde{E}^2-1)^2}{\tilde{E}^2}\int_{-\infty}^{\infty} 1 - 4\tanh^2\left(\frac{y}{\ell}\right) + 2\tanh^4\left(\frac{y}{\ell}\right) dy. \tag{6}$$

The elastic energy excess U_{BL} of the BL wall is obtained by substracting from the expression (6) the energy $\mathcal{F}_2$ of a uniform Fréedericksz domain [2]:

$$\mathcal{F}_2 = -\frac{K\pi^2}{4d}\frac{(\tilde{E}^2-1)^2}{\tilde{E}^2}\int_{-\infty}^{\infty} dy. \tag{7}$$

$U_{BL}=\mathcal{F}_1-\mathcal{F}_2$ is finally written [22]

$$U_{BL} = \frac{2^{3/2}}{3}K\pi\frac{(\tilde{E}^2-1)^{3/2}}{\tilde{E}^2}. \tag{8}$$

The elastic energy per unit length of the disclination bent region U_β, is composed of two terms of different origins: the core energy $U_c \approx 2K$ of the two mobile line segments (AB and $B'A'$) and the bulk elastic energy due to the disclinations. To compute the elastic energy of a disclination in presence of an electric field, we compare the elastic torque per unit surface associated to an isolated disclination ($\Gamma_{el}=K/r$, where r is the distance from the disclination) to the dielectric torque ($\Gamma_E=K/\xi_E$, where $\xi_E=(dE_F)/(\pi E_C)$ is the electric coherence length). The term Γ_{el} prevails in a cylinder $\mathcal{C}$ of radius ξ_E around the disclination, while Γ_E governs the director behavior outside $\mathcal{C}$. At the first order, the elastic energy is the sum of the defect elastic energy U_1 inside $\mathcal{C}$ in absence of a field [2] and the dielectric energy U_2 outside $\mathcal{C}$ for a director parallel to the electric field. We obtain U_1 by integrating the elastic energy associated to a disclination on a cylinder of radius ξ_E:

$$U_1 = \frac{K}{2}\pi\ln\frac{\xi_E}{\xi}, \tag{9}$$

where the cutoff length ξ is the nematic-isotropic coherence length [23,24]. To obtain the expression (9), we have neglected the anchoring contribution to the disclination elastic energy [24,25]. The second term U_2 is written

$$U_2 = -\frac{E^2\epsilon_0\epsilon_a}{2}\int_{-\xi_E}^{\xi_E}\int_{\xi_E}^{d-\xi_E}\sin^2\theta\, dy\, dz. \tag{10}$$

In the limit $\xi_E \ll d$ and by considering a saturated director texture with $\hat{\mathbf{n}}$ parallel to the electric field ($\theta=\pi/2$), we obtain

$$U_2 = -K\pi\tilde{E}. \tag{11}$$

The sum of the three contributions U_c, U_1, U_2, gives the total energy per unit length:

$$U_\beta = K\pi\left(\frac{1}{2}\ln\frac{d}{\pi\tilde{E}\xi} + \frac{2}{\pi} - \tilde{E}\right). \tag{12}$$

The resulting driving elastic force [Eq. (1)] is

$$F_{el} = U_\beta - U_{BL} = -\frac{2^{3/2}}{3}K\pi\frac{(\tilde{E}^2-1)^{3/2}}{\tilde{E}^2} + K\pi\left(\frac{1}{2}\ln\frac{d}{\pi\tilde{E}\xi} + \frac{2}{\pi} - \tilde{E}\right). \tag{13}$$

Let us now compare the experimental data to the model predictions. The value of the stabilization field E_C is given by the implicit equation $U_{BL}=U_\beta$

$$d = \xi\pi\tilde{E}_C\exp\left[2\left(\tilde{E}_C - \frac{2}{\pi} + \frac{2^{3/2}}{3}\frac{(\tilde{E}_C^2-1)^{3/2}}{\tilde{E}_C^2}\right)\right]. \tag{14}$$

Contrary to E_c (see Fig. 10), $\tilde{E}_C$ should be almost constant with the temperature because ξ displays only a very slight temperature dependence. This prediction agrees with the experimental results shown in Fig. 11. Moreover the dependence of $\tilde{E}_C$ on the cell thickness shown in Fig. 12 is well reproduced by the model with $\xi=2.2\pm1.1$ nm, which is in good agreement with the literature values [23].

Concerning the dynamics, the driving elastic force is balanced by a viscous force F_v mainly due to the director reorientation in the cylinder $\mathcal{C}$ around the straight BB' part. In this limit, by using the notation of Cladis *et al.* [6], the viscous force acting on the line is written

$$F_v = 2bv\, d\zeta, \tag{15}$$

where $\zeta = \gamma_1 - \alpha_2^2/[2(\eta_\beta - \gamma_2)]$ [6] is an effective viscosity which takes into account in an empiric way the backflow effects. The parameters γ_1, α_2, η_β, and γ_2 are related to the Leslie coefficients. The number b of order unity depends on the details of the energy dissipation in the cylinder $\mathcal{C}$. At the first order, we expect that the effect of the experimentally observed weak bending of the part BB' just renormalizes the drag force (15) or the empiric effective viscosity ζ. We then obtain the velocity

$$v = \frac{K\pi}{2b\zeta d}\left(\frac{2^{3/2}}{3}\frac{(\tilde{E}^2-1)^{3/2}}{\tilde{E}^2} - \frac{1}{2}\ln\frac{d}{\pi\xi\tilde{E}} - \frac{2}{\pi} + \tilde{E}\right). \tag{16}$$

Numerical calculations show that v is almost linear in $(\tilde{E} - \tilde{E}_C)$ in the range of our measurements $\tilde{E}=1$–4. A Taylor expansion of Eq. (16) around $\tilde{E}=\tilde{E}_C$ gives

$$v = \alpha E_F(\tilde{E} - \tilde{E}_C), \tag{17}$$

with a velocity susceptibility to the electric field α given by

$$\alpha = \left.\frac{\partial v}{\partial E}\right|_{E=E_C} = \frac{K\pi}{2b\zeta V_F}\left[\frac{2^{3/2}}{3}\frac{(\tilde{E}_C^2-1)^{1/2}(\tilde{E}_C^2+2)}{\tilde{E}_C^3} + \frac{1}{2\tilde{E}_C} + 1\right], \tag{18}$$

where $V_F = E_F d$.

Let us compare now the measured values of the susceptibilities α with the expression (18). The value α (Fig. 13) does not depend on the cell thickness as expected from Eq. (18). Using the known 5CB material parameters K [26], ϵ_a [27], and ζ [28], we have obtained $b=1.22$ (plain line in Fig. 13). The coefficient b depends slightly on temperature. From the temperature dependence of α (Fig. 14), we have found $0.8 < b < 1.2$ in the explored temperature range. b remains of the order of the unity which means that our model captures the main properties of the disclination dynamics. We can conclude that our model is in a good agreement with the experimentally measured electric field induced deformation dynamics of a nematic disclination.

V. CONCLUSIONS

We have studied the deformation dynamics of a single $1/2$ nematic disclination under an external electric field. Disclinations pair of opposite strength are obtained by a rapid quench from the isotropic phase into the nematic phase. The nematic phase is confined in a cell with uniform director oriented along the two parallel planar easy axes of the substrates. In each pair, disclinations straight and orthogonal to the substrates are connected by a costly anchoring surface wall. The pair annihilation is induced by the anchoring energy excess stored in this surface wall. Before the disclination disappearance, a disorienting electric field is applied. Above the Fréedericksz transition, domains appear corresponding to one of the twofold degenerate textures separated by a bulk Brochar-Léger wall. Segments of the Brochard-Léger wall systematically connect the disclinations. By increasing the electric field amplitude, the annihilation dynamics is dampened. At a critical field $E_C \approx 2E_F$, the disclinations are immobilized: the anchoring dominated annihilation force on each disclination is now counterbalanced by a generalized elastic force due to the electric-field-induced director texture. Depending on the sample temperature and on the electric field amplitude different behaviors are measured.

At low temperature ($\Delta T > 2\,^\circ$C) and under an electric field amplitude close to E_C, the disclination is strongly pinned on each substrate. If $E > E_C$ the line defect bends. The bending profile is characterized by two parts, parallel and close to the substrates, connected with a third part bent in the bulk. This bent disclination region growths at the expense of the Brochard-Léger wall, in a process corresponding to a conversion of the Brochard-Léger wall into the two parts of the disclination parallel to the substrate. This behavior is reminiscent of the field-induced disclination nucleation in the *pincement* phenomenon. The field values where it appears compare well with the ones measured for *pincement*.

The line deformation dynamics is measured for electric field close to E_C. This dynamics is obtained from the measurement of the position of the line bending inversion point. The inversion point velocity has been measured as function of the electric field amplitude, cell thickness and sample temperature. An elastic model has been elaborated that accounts for the experimental results.

In the future, the electric-field-induced disclination behavior will be extended to the high temperature regime. Experiments currently in progress show that, in this temperature range, disclinations are weakly pinned on the substrates and the resulting dynamics is much more complex.

In conclusion, we show that a line pinned on the two confinement substrates can be deformed in a controlled way by an external electric field. These results open further possibilities to the manipulation of individual topological defects in a nematic liquid crystal.

[1] M. Kleman, Rep. Prog. Phys. **52**, 555 (1989).
[2] P. G. de Gennes and J. Prost, *The Physics of Liquid Crystals*, 2nd ed. (Clarendon Press, Oxford, 1993).
[3] M. Kleman, *Lines and Walls in Liquid Crystals* (Wiley, New York, 1983).
[4] M. Kleman and O. Lavrentovich, *Soft Matter Physics: An Introduction* (Springer, New York, 2003).
[5] I. Chuang, N. Turok, and B. Yurke, Phys. Rev. Lett. **66**, 2472 (1991).
[6] P. E. Cladis, W. van Saarloos, P. L. Finn, and A. R. Kortan,

Phys. Rev. Lett. **58**, 222 (1987).
[7] A. Bogi, P. Martinot-Lagarde, I. Dozov, and M. Nobili, Phys. Rev. Lett. **89**, 225501 (2002).
[8] F. Brochard, J. Phys. (Paris) **33**, 607 (1972).
[9] L. Leger, Mol. Cryst. Liq. Cryst. **24**, 33 (1973).
[10] A. Stieb, G. Baur, and M. Meier, J. Phys. (Paris) **36**, C1 (1975).
[11] K. S. Krishnamurthy and R. Balakrishnan, Liq. Cryst. **29**, 383 (2002).
[12] J. Ignès-Mullol, J. Baudry, L. Lejcek, and P. Oswald, Phys. Rev. E **59**, 568 (1999).
[13] M. Mihailovic and P. Oswald, J. Phys. (Paris) **49**, 1467 (1988).
[14] Y. Galerne, J. Itoua, and L. Liebert, J. Phys. (Paris) **49**, 681 (1988).
[15] C. Chevallard, M. Clerc, P. Coullet, and J. Gilli, Europhys. Lett. **58**, 686 (2002).
[16] B. A. Belyaev, N. A. Drokin, V. F. Shabanov, and V. N. Shepov, Mol. Cryst. Liq. Cryst. Sci. Technol., Sect. A **366**, 2157 (2001).
[17] I. I. Smalyukh, S. V. Shiyanovskii, and O. D. Lavrentovich, Chem. Phys. Lett. **336**, 88 (2001).
[18] S. V. Shiyanovskii, I. I. Smalyukh, and O. D. Lavrentovich, in *Defects in Liquid Crystals: Computer Simulations, Theory and Experiments*, edited by O. D. Lavrentovich, P. Pasini, C. Zannoni, and S. Zumer, NATO Science Series (Kluwer Academic Publishers, Dordrecht, 2001), pp. 229–270.
[19] M. Kleman and O. Lavrentovich, *Soft Matter Physics: An Introduction* (Springer, New York, 2003), Chap. 12.4.1.
[20] C. Chevallard, Ph.D. thesis, Université de Nice, 1985 (unpublished).
[21] At large fields $E \approx E_C = 2E_F$ this approximation is still relevant. If we compare the exact free energy and the one obtained by taking into account only the first mode of the θ expansion, the relative error remains quite small ($\sim 16\%$).
[22] S. Chandrasekhar and G. S. Ranganath, Adv. Phys. **35**, 507 (1986).
[23] E. B. Priestley, P. J. Wojtowicz, and P. Sheng, *Introduction to Liquid Crystals* (Plenum, New York, 1974), Chap. 10, pp. 151-161.
[24] For a surface-disclination distance of a few micrometers as measured in Fig. 9 (parts AB and AB′), the disclination elastic energy change due to the anchoring remains relatively small ($\sim 10\%$) compared to the one in Eq. (9).
[25] R. B. Meyer, Solid State Commun. **12**, 585 (1973).
[26] J. D. Bunning, T. E. Faber, and P. L. Sherrel, J. Phys. I **42**, 1175 (1991).
[27] B. R. Ratna and P. Shashidhar, Mol. Cryst. Liq. Cryst. **42**, 113 (1977).
[28] K. Skarp, S. Lagerwall, and B. Stebler, Mol. Cryst. Liq. Cryst. **60**, 215 (1980).